



ELSEVIER

Computerized Medical Imaging and Graphics 28 (2004) 39–50

**Computerized  
Medical Imaging  
and Graphics**

[www.elsevier.com/locate/compmedimag](http://www.elsevier.com/locate/compmedimag)

## Image analysis techniques for characterizing disc space narrowing in cervical vertebrae interfaces

Pavan Chamorthy<sup>a</sup>, R. Joe Stanley<sup>a,\*</sup>, Gregory Cizek<sup>b</sup>, Rodney Long<sup>c</sup>, Sameer Antani<sup>c</sup>, George Thoma<sup>c</sup>

<sup>a</sup>Department of Electrical and Computer Engineering, University of Missouri-Rolla, Rolla, MO 65409, USA

<sup>b</sup>Excel Imaging, St Louis, MO, USA

<sup>c</sup>Communications Engineering Branch, National Library of Medicine, Bethesda, MD, USA

Received 23 May 2003; accepted 10 October 2003

### Abstract

Image analysis techniques are introduced for evaluating disc space narrowing of cervical vertebrae interfaces from X-ray images. Four scale-invariant, distance transform-based features are presented for characterizing the spacing between adjacent vertebrae. *K*-means and self-organizing map clustering techniques are applied to estimate the degree of disc space narrowing using a four grade (0–3) scoring system, where 0 and 3 represent normal spacing and significant narrowing, respectively. For a data set of 294 vertebrae interfaces, experimental results yield average correct grade assignment of greater than 82.10% for each of the four grades using a one grade window around the correct grade.

© 2003 Elsevier Ltd. All rights reserved.

**Keywords:** Degenerative disk disease; Disc space narrowing; Image processing; Cervical spine disorders; *K*-means; Self-organizing maps

### 1. Introduction

Osteoarthritis is the one of the most common forms of arthritis and is often associated with ageing. Osteoarthritis affects more than 16 million Americans [1]. Osteoporosis is a disease that is characterized by low bone mass and structural deterioration of bone tissue, which may result in fragile bones and an increased susceptibility to hip, spine and wrist fractures [2]. Around 70,000 vertebral fractures occur annually in the US due to osteoporosis [2]. Radiographs of the spine are an important tool to assist radiologists in estimating and assessing osteoarthritis, spondylosis, and other disc degenerative related diseases. Osteophytes ('bony growths'), disc space narrowing, and subluxation are typical radiographic hallmarks characterizing those diseases. Imaging techniques like Magnetic Resonance Imaging (MRI), CAT scan or Computer Tomography (CT), myelogram and discogram can also be used to obtain detailed information on cervical spine images. The Lister Hill National Center for Biomedical Communications, an R&D division of the National Library

of Medicine (NLM), has built a Web-based Medical Information Retrieval System (WebMIRS) to permit Internet access to databases of X-ray images and associated text data from the National Health and Nutrition Examination Surveys (NHANES) [3]. Part of the WebMIRS initiative was to study the feasibility of computer-based techniques to detect cervical spine disorders. The NHANES database has a collection of radiographs of the cervical spine for the study of degenerative disorders like osteoarthritis in the US.

Vertebral morphometry is a commonly used technique to quantitatively evaluate features related to spine structure, injury, and pathology. In particular, measuring morphometric vertebral deformity is often used in clinical trials for assisting in the diagnosis and follow-up of fractures. Measurement techniques include conventional rulers and calipers [4–8] and digitizing tablets [9–12]. Morphometric analysis has encompassed radiographic diagnosis of vertebral fractures based on subjective visual assessment and arbitrarily assessed reductions in vertebral heights [13–15]. Prior studies have utilized vertebral dimensions to establish normal ranges using anterior and posterior vertebral height, percent reduction of anterior compared to posterior height of

\* Corresponding author. Tel.: +15733416896; fax: +15733414532.

the same vertebra, the difference in vertebral height of adjoining vertebrae, vertebral width, wedge angle and vertebra angle [4]. Other techniques such as quantitative computed tomography (QCT) [16], dual photon absorptiometry (DPA) [17] and dual energy radiography [18] facilitate accurate assessment of bone mineral content and spine density.

Usual disc modifications consist of disk space narrowing, disc space enlargement, intervertebral disc calcifications, intervertebral disc prolapse and signal modification in MRI [19]. There are numerous factors that contribute to disc degeneration, including age [20], gender [21], extreme physical activity [22], among others. Disc space narrowing may be associated with nerve root compression and can cause pain. The reduction of the foraminal area is directly proportional to the amount of disc narrowing [23]. Estimation of disc space narrowing can help predict some other spine anomalies. For example, substantial joint space narrowing is often associated with a severe degree of subluxation [24].

There are seven cervical vertebrae (C1–C7) in the human body. Fig. 1 presents a cervical X-ray image example with arrows pointing to the vertebrae interfaces between C3–C4, C4–C5, C5–C6 and C6–C7. Intervertebral disc spacing is evaluated in this research for vertebrae interfaces between C3–C4, C4–C5 and C5–C6. The Communications Engineering Branch of the National Library of Medicine developed the Online Digital Atlas Version 2.0 in 2000 to provide a digital reference source to assist with the interpretation of cervical and lumbar

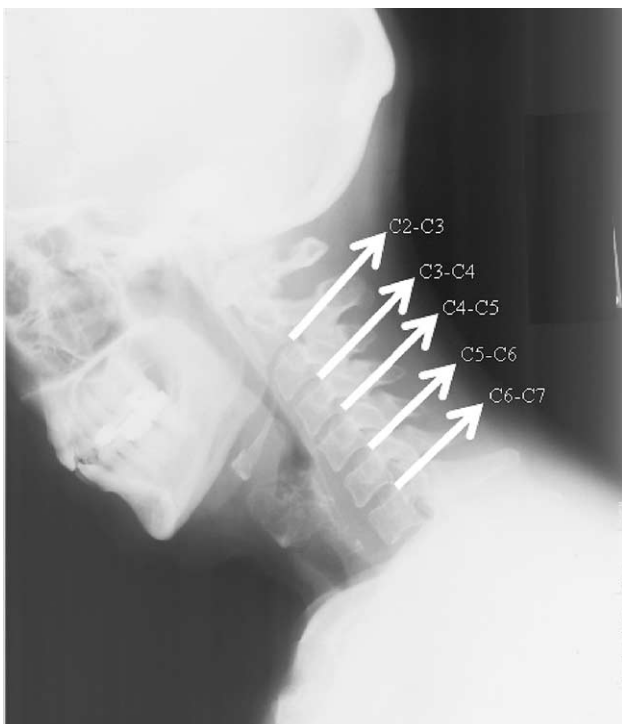


Fig. 1. An example of a cervical spine X-ray image. Arrows highlight the vertebrae interfaces for C3–C4, C4–C5, C5–C6, and C6–C7.

vertebrae in X-ray images [25]. Images used in the development of the Atlas tool were chosen from 17,000 digitized X-ray films that were obtained through the National Center for Health Statistics (NCHS) from 1976 to 1980. Medical experts from the National Institute of Arthritis, Musculoskeletal, and Skin Diseases (NIAMS) and the NIH Clinical Center selected films from which high quality photographs were obtained and given to three rheumatologists for osteoarthritis-related features. Each of the rheumatologists scored each image on a scale of 0–3, with 0 indicating normality and 3 maximum abnormality, for anterior osteophytes and disc space narrowing. The smaller the disk space, the greater is the severity of the narrowing for the vertebrae pair under consideration. For subluxation, only a score of 0 or 1 for absence or presence was used. The rheumatologists used the Atlas of Standard Radiographs of Arthritis [26] as a reference to maintain consistent interpretation. Fig. 2 presents image examples included in the Atlas tool for each of the grades 0–3 for disc space narrowing between adjacent cervical vertebrae.

The development of automated/semi-automated approaches is relatively recent for cervical and lumbar spine and other radiographic image analysis for characterizing features related to osteoarthritis. In previous research, computer-assisted image analysis techniques were investigated for radius of curvature and boundary gradient features to detect anterior osteophytes in cervical vertebrae [27]. Automated image analysis techniques have also been applied to evaluate herniation classification and geometry in the diagnosis of lumbar herniated inter-vertebral disc [28]. Computer-assisted techniques have been explored using the radiographs of the knee for monitoring osteoarthritis progression based on minimum joint space measurement between edges of the femoral condyle and the tibial plateau [29].

This paper introduces image analysis and pattern recognition techniques to estimate the degree of intervertebral disc spacing between adjacent cervical vertebrae from X-ray images. In this research, computer-assisted techniques are investigated for disc space narrowing assessment in cervical vertebrae interfaces. Image processing techniques are presented for determining an equidistant separator segment between adjacent vertebrae to facilitate feature calculations. The equidistant separator segment between adjacent vertebrae provides the basis for determining the spacing between those vertebrae. Four scale invariant features are introduced based on the size of the adjacent vertebrae and the ‘distance’ between those vertebrae based on the equidistant separator. Clustering approaches using *K*-means and self-organizing maps (SOMs) are explored for feature evaluation. Disc space narrowing grade assignment based on the four grade system (0–3) is performed using an exact grade assignment and a window of 1 grade assignment for assessing the algorithms developed. The remainder of the paper is organized in

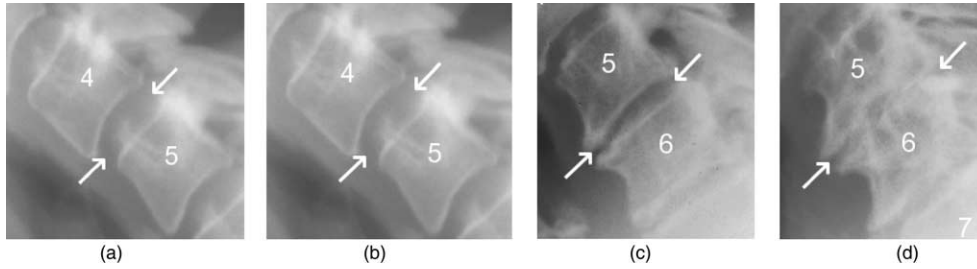


Fig. 2. Example of various grades of disk space narrowing in cervical spine images obtained from the Online Digital Atlas Version 2.0. (a) Grade 0. (b) Grade 1. (c) Grade 2. (d) Grade 3.

the following sections: (1) algorithm for manual vertebra segmentation, (2) algorithm for determining separator between adjacent vertebrae, (3) size-invariant features for quantifying the vertebrae interface spacing, (4) clustering technique for disc space narrowing grade assignment, (5) experiments performed, (6) experimental results and discussion, and (7) summary of results obtained.

## 2. Methods

### 2.1. Vertebrae interface dataset

In this research, disc space narrowing was evaluated for adjacent cervical vertebrae from 98 cervical spine X-ray images. The vertebra interfaces examined from this data set include C3–C4, C4–C5, C5–C6 and C6–C7. An expert radiologist truthed the cervical vertebrae data set using a four grade system (grades 0–3), where grade 0 reflects normal spacing and grade 3 represents abnormal disc space narrowing. To assist the radiologist in vertebrae truthing, the radiologist used the grade assignment examples for disc space narrowing from the Online Digital Atlas Version 2.0 developed by the Communications Engineering Branch of the National Library of Medicine. The vertebrae interfaces C3–C4, C4–C5 and C5–C6 were clearly observable, but the interfaces for C6–C7 were not clear for many images in the data set. Thus, the vertebra interfaces C3–C4, C4–C5 and C5–C6 were considered for this research, providing a total data set of 294 interfaces (three interfaces per image for 98 images). Table 1 shows the distribution of these records among various grades (0–3). Let  $L_0$ ,  $L_1$ ,  $L_2$  and  $L_3$  denote the number of vertebrae interfaces with grades 0–3, respectively. From Table 1,  $L_0 = 59$ ,  $L_1 = 145$ ,  $L_2 = 59$  and  $L_3 = 31$ , respectively.

Table 1  
Summary of data set used for disc space narrowing prediction for cervical vertebra interfaces for C3–C4, C4–C5, and C5–C6

Level	Grade 0	Grade 1	Grade 2	Grade 3	Total
C3–C4	30	49	13	6	98
C4–C5	18	54	15	11	98
C5–C6	11	42	31	14	98
Total	59	145	59	31	294

### 2.2. Overview of disc space narrowing prediction algorithm

In this research, four distance transform-based, size-invariant features are investigated for categorizing varying grades of disc space narrowing. The algorithm for adjacent vertebra interface analysis is presented in Fig. 3. The initial step involves manually segmenting each vertebra within the cervical spine X-ray images. The second step of the algorithm is to perform image processing operations to automatically determine an equidistant separator segment between adjacent vertebrae to characterize the vertebrae interface. The fourth step is to compute size-invariant features based on the Euclidean distance found along the equidistant separator and the size of the vertebrae. The final step is to categorize the grade of disc grade narrowing using a two-tier pattern recognition approach. The two-tier technique integrates *K*-means clustering and SOMs.

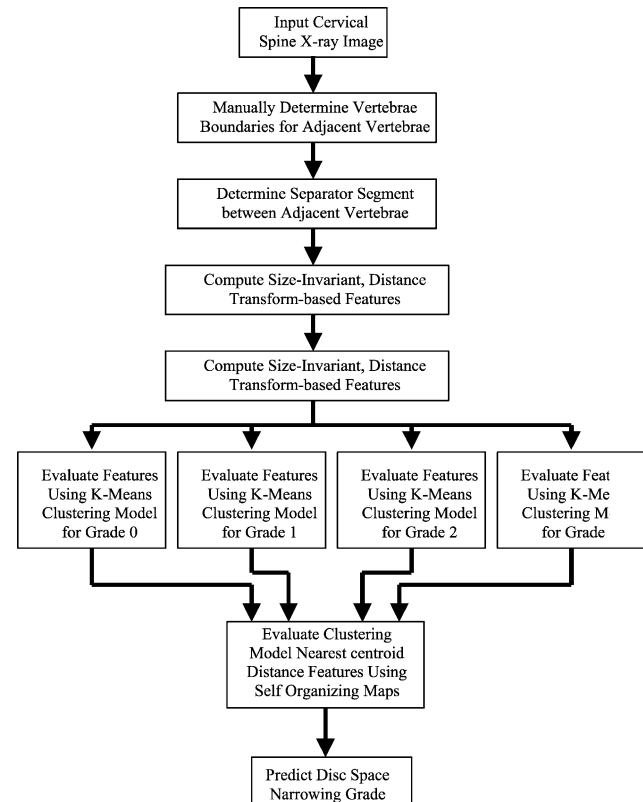


Fig. 3. Flow chart showing the disc space narrowing assessment process for pair of adjacent vertebrae.

The following sections present the different algorithm steps in detail.

### 2.3. Vertebra boundary determination

For the cervical spine X-ray images used in this research, an expert radiologist identified and marked 7–9 points along the vertebra's boundary. The radiologist marked the top and bottom points of the anterior and posterior sides, the midpoints of the top and bottom sides, the anterior midpoint, and up to two points near the anterior corners where osteophytes (if any) were located. For vertebra segmentation, vertebral boundary points were manually chosen and a second order B-spline algorithm [30] was used to connect the points to generate a closed boundary. A B-spline approach has been applied to disc boundary approximation for diagnosing lumbar herniated inter-vertebral disc [28].

In order to assist with manual vertebra boundary point selection, an edge magnitude image was determined to assist in determining vertebrae boundaries. The expert radiologist selected points were superimposed onto the edge magnitude image to facilitate vertebral boundary point selection. Based on the observations from several edge detectors, the magnitude images obtained from applying the Kirsch operator [31] reasonably highlighted the vertebra boundary. Based on experimentation, approximately 55 manually-chosen points provided a reasonable vertebral boundary representation for feature analysis. Fig. 4 presents an edge magnitude image example (cropped to only contain the vertebrae region of the original X-ray image) with the radiologist points superimposed (a) and a reference vertebra containing the selected positions along the vertebra boundary that the radiologist would label (b). Fig. 4 (a) provides an example image used to assist in the manual point selection process for each vertebra. The arrows in Fig. 4 (a) point to two radiologist-provided points. Points 8 and 9 in Fig. 4 (b) represent anterior osteophytes that might

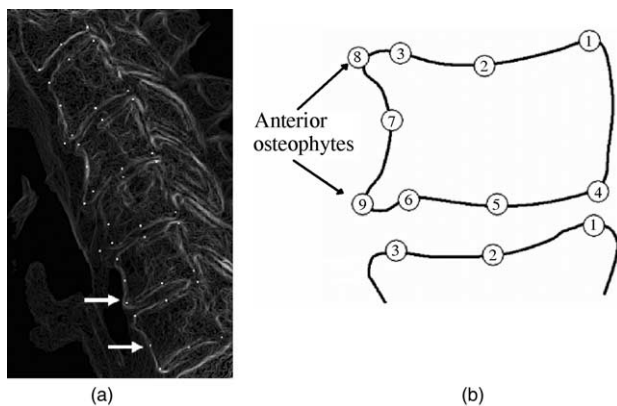


Fig. 4. Image examples of aides to assist with manual vertebra boundary determination. (a) Edge magnitude image with radiologist selected points superimposed. (b) Labeled points that the expert radiologist selects to characterize a vertebra. Points 8 and 9 are locations for anterior osteophytes.

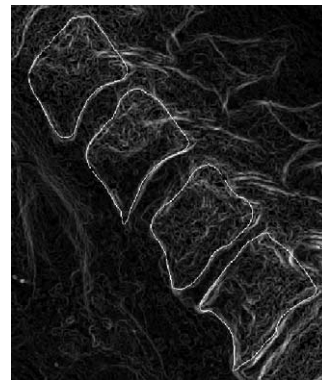


Fig. 5. Image example of vertebrae boundaries obtained using the manual point selection and B-spline procedure. Vertebrae boundaries have been superimposed onto the corresponding edge magnitude image.

be present at the lower and upper anterior portions of the vertebra. Fig. 5 shows an image illustration of vertebrae boundaries determined from the manual point selection process and B-Spline algorithm that have been superimposed onto the corresponding edge magnitude image.

### 2.4. Algorithm for determining equidistant separator segment between adjacent vertebrae

The algorithm for determining the equal distance separator between adjacent vertebrae uses the manually segmented vertebrae within an X-ray image. For the cervical X-ray images examined, vertebrae C3–C6 were manually segmented using the procedure described in Section 2.3. The algorithm to find the equidistant separator between adjacent vertebrae is presented in Fig. 6. Let  $I$  denote the binary X-ray image containing all vertebra boundaries. The adjacent vertebrae are identified for which to perform disc space narrowing analysis. A raster scan of the image is used to determine the locations of the vertebrae (C3–C6) within the image. Let  $C_i$  and  $C_j$  denote adjacent vertebrae for  $3 \leq i \leq 5$ ,  $4 \leq j \leq 6$  and  $i < j$ . For adjacent vertebrae  $C_i$  and  $C_j$ , find the leftmost, topmost, rightmost and bottommost points, forming a bounding box region. Let  $(R_0, C_0)$ ,  $(R_0, C_1)$ ,  $(R_1, C_0)$ , and  $(R_1, C_1)$  denote the corner points of the bounding box, where  $C_0$  is the leftmost column,  $C_1$  is the rightmost column,  $R_0$  is the topmost row, and  $R_1$  is the bottommost row. The interiors of the adjacent vertebrae are filled, with areas  $A_i$  and  $A_j$  for vertebrae  $C_i$  and  $C_j$ , respectively. The bounding box region containing the filled adjacent vertebrae is inverted so that the vertebrae

*Manually obtain vertebrae boundaries within x-ray image*  
*Find adjacent vertebrae*  
*Create region of interest containing adjacent vertebrae*  
*Fill vertebrae interiors*  
*Invert filled vertebrae to highlight surrounding regions*  
*Compute distance transform "image" from surrounding regions to nearest vertebra*  
*Compute edge magnitude and direction "images" from distance transform "image"*  
*Compute histogram of edge directions*  
*Determine separator between adjacent vertebrae*

Fig. 6. Algorithm to find the equidistant separator between adjacent vertebrae.

surrounding region becomes the region of interest. The distance transform [32] is applied to the surrounding region for determining the distance to the nearest vertebra. The distance transform is computed using the rounded value of the Euclidean distance. Let  $D$  represent the distance image over the adjacent vertebrae region of interest, where  $D(x, y)$  is bounded by  $C_0 \leq x \leq C_1$  and  $R_0 \leq y \leq R_1$ .

The equidistant separator corresponds to the local maxima contour from the distance transform image. The contour is determined based on Kirsch edge operator [31]. The Kirsch operator is a  $3 \times 3$  gradient-based operator that provides the gradient magnitude and corresponding gradient direction, with the gradient direction determined in increments of  $45^\circ$ . Let  $K$  denote the gradient magnitude computed at each pixel based on the distance transform computed within the adjacent vertebrae surrounding region. Let  $G$  represent the corresponding gradient direction from the Kirsch operator at each pixel within the adjacent vertebrae surrounding region. Note that the gradient direction is perpendicular to the edge, i.e. contour. The local maximum region in the distance transform image corresponds to the contour separating the adjacent vertebrae. A histogram of the direction component of the Kirsch edge detector output is determined to identify the edge direction with highest frequency ( $\text{dir}_{\max}$ ). This edge direction corresponds to the perpendicular direction of largest contour in the region surrounding the adjacent vertebrae. The largest contour represents the separator between adjacent vertebrae. Because the separator between adjacent vertebrae is not necessarily linear, the direction of the separator ( $\text{dir}_{\max}$ ) is relaxed to include up to one adjacent direction on either side of  $\text{dir}_{\max}$  ( $\pm 45^\circ$  from  $\text{dir}_{\max}$ ). Let  $S$  denote the separator thresholded image with  $S$  defined as

$$S(x, y) = \begin{cases} 1 & \text{if } \text{dir}_{\max} - 1 \leq G(x, y) \leq \text{dir}_{\max} + 1 \text{ and } K(x, y) \geq 5 \\ 0 & \text{otherwise} \end{cases},$$

where  $C_0 \leq x \leq C_1$  and  $R_0 \leq y \leq R_1$ . Noise points are generated from the relaxed gradient direction ( $\text{dir}_{\max}$ ). Without the relaxation, potential holes result in the extracted contour. Morphological closing [33] with a small structuring element disk of radius 2 is performed on  $S$  to facilitate gap and hole removal in the extracted contour. Let  $Z$  denote the resulting closed separator thresholded image  $S$ .

The noise points are found using a template matching approach based on the most frequently occurring gradient direction found from  $S$ . Specifically, a  $3 \times 3$  mask in the direction of  $\text{dir}_{\max}$  is applied to  $Z$ . An example of the mask applied at each pixel within  $Z$  is given as follows. Fig. 7(a) shows a  $3 \times 3$  mask with the gradient directions labeled 1–8. For illustrative purposes, suppose that index 3 (shown in bold on Fig. 7) represents  $\text{dir}_{\max}$  found from the histogram of direction values. Fig. 7(b) shows the resulting  $3 \times 3$  hit mask that would be applied to  $Z$  in determining the noise pixels. The noise image ( $Y$ ) output from the hit mask

4	<b>3</b>	2
5	( )	1
6	7	8

(a)

0	1	0
1	(1)	1
1	1	1

(b)

Fig. 7. Example of the  $3 \times 3$  mask applied at each pixel in the intermediate separator image  $Z$  for noise removal. (a)  $3 \times 3$  mask with the gradient directions labeled 1–8. (b)  $3 \times 3$  hit mask that would be applied to  $Z$  based on index 3 (shown in bold) representing  $\text{dir}_{\max}$  found from the histogram of direction values.

is determined as follows

$$Y(x, y) = \begin{cases} 1 & \text{if hit mask completely matches } Z \text{ at } (x, y) \\ 0 & \text{otherwise} \end{cases},$$

where  $C_0 \leq x \leq C_1$  and  $R_0 \leq y \leq R_1$ .  $Y$  is dilated by a  $3 \times 3$  circular structuring element (four corners are zeros) for region-growing the noise region, with the resulting image denoted as  $E$ . Let  $B$  represent the difference image between  $S$  and  $E$  such that  $B(x, y) = Z(x, y) - E(x, y)$  for  $C_0 \leq x \leq C_1$  and  $R_0 \leq y \leq R_1$ .  $B$  contains several potential vertebrae separator objects. Using connected component labeling [34], the area is computed for each of the separator objects. The object with the largest area is selected as the vertebrae separator segment.

After the separator segment has been found, the next step is to restrict separator to lie approximately between the adjacent vertebrae. The centroid of each adjacent vertebra is computed. Let  $d_{\text{cen}}$  denote the Euclidean distance between the centroids of  $C_i$  and  $C_j$ . Using the centroid positions, the leftmost and rightmost column positions of each vertebra are determined. From this process, coordinate positions are obtained on the left side and right side boundaries of each vertebra. Equations for the lines through the adjacent vertebra leftmost points and through the rightmost points are derived. The points on the separator segment to the right of the leftmost line and to the left of the rightmost line define the portion of the separator to be used for disk space narrowing assessment. The last step is to skeletonize the separator object to obtain the final vertebrae separator ( $V$ ). The separator represents an equidistant segment between the adjacent vertebrae because the separator represents the contour between adjacent vertebrae based on the distance transform. The separator  $V$  provides an equidistant separator between adjacent vertebrae that represents approximately half the distance (Euclidean) between the adjacent vertebrae. The separator  $V$  provides a binary mask of the equidistant separator between the adjacent vertebrae.

### 2.5. Disk space narrowing feature calculation

Once the vertebra separator ( $V$ ) has been found, disk space narrowing features are computed. In this research, size-invariant, distance transform-based features are computed using the mask  $V$ . Let the mean and minimum distance along the separator be denoted as  $X_{\text{mean}}$  and  $X_{\text{min}}$ , respectively, where  $X_{\text{mean}} = (\sum_{(x,y) \in V} D(x, y)) / (A_V)$ ,

$X_{\min} = \min_{(x,y) \in V} (D(x,y))$  and  $A_V$  represents the ‘area’ of the separator region  $V$ . The four size-invariant features include: (1) the ratio  $M$  of the minimum Euclidean distance spacing to the maximum of the square root of  $A_i$  and  $A_j$  ( $M$ ), (2) the ratio  $O$  of the mean Euclidean distance spacing to the maximum of the square root of  $A_i$  and  $A_j$  ( $O$ ), (3) the ratio  $P$  of the mean Euclidean distance spacing to the minimum of the square root of  $A_i$  and  $A_j$  ( $P$ ) and (4) the ratio  $R$  of the mean Euclidean distance spacing to the centroid distance between  $C_i$  and  $C_j$  ( $R$ ). Mathematically, the features are computed as  $M = (X_{\min})/(\max(\sqrt{A_i}, \sqrt{A_j}))$ ,  $O = (X_{\text{mean}})/\max(\sqrt{A_i}, \sqrt{A_j})$ ,  $P = (X_{\text{mean}})/(\min(\sqrt{A_i}, \sqrt{A_j}))$  and  $R = (X_{\text{mean}})/(d_{\text{cen}})$ , respectively. The intent with these features was to evaluate the spacing between adjacent vertebrae relative to the size of the adjacent vertebrae.

### 2.6. Disc space narrowing grade assignment procedure

For each adjacent vertebra pair within an X-ray image, the features  $M, O, P$  and  $R$  are computed. From Table 1, there are many more vertebrae pairs with disc space narrowing grades of 0 and 1 than there are vertebrae pairs with grades of 2 and 3. Accordingly, the technique developed for automatically assigning the disc space narrowing grade accommodates for the variation of training data between the various grade classes. Furthermore, the disc space narrowing grades 0–3 provide an increasing scale for disc space abnormalities with 0 as normal and 3 as significant disc space narrowing. The distinction between consecutive grade assignments is often difficult to visually determine. The automated approach investigated for disc space narrowing assignment compares the capability to perform actual grade assignment to window grade assignment, i.e. grade assignment within one grade of the expert radiologist assessment.

A two-tier pattern recognition approach was investigated for assigning grades of disc space narrowing between adjacent vertebrae. The two-tiers include inputting the feature vector ( $M, O, P, R$ ) for each vertebra pair into a  $K$ -means clustering algorithm [35] which provides outputs that are input to a SOM [36]. The outputs of the SOM provide a disc space narrowing grade assignment. The following sections present the two-tier pattern recognition method. For evaluating the features presented using the two-tier pattern recognition technique overviewed, the data set shown in Table 1 is divided into 80% of the adjacent vertebrae cases for each grade for algorithm training and the remaining 20% for algorithm testing.

### 2.7. $K$ -means clustering and nearest centroid algorithm

In the initial step of disc space narrowing grade assignment, separate  $K$ -means clustering models are developed for each grade. The inputs to each of the  $K$ -means models are the features  $M, O, P$ , and  $R$  for each adjacent vertebrae pair. For each  $K$ -means model, the training data

for the corresponding grade are used for determining the cluster centers. Using the training data for each grade, the mean and standard deviation of each feature is computed. Let  $\mu_{0,M}$  and  $\sigma_{0,M}$  denote the mean and standard deviation for feature  $M$  computed from the training data for grade 0. Similar designations are given for the means and standard deviations for grades 1–3. For the training data, the feature vectors input to the  $K$ -means model for each grade are normalized by subtracting the corresponding mean feature value and dividing by the corresponding standard deviation value. The number of clusters used for the model for each grade was determined empirically. Let the number of clusters in each grade be denoted as  $N_0, N_1, N_2$  and  $N_3$  for grades 0–3, respectively. Using the training data, the cluster centers are determined for each grade.

For disc space narrowing grade assignment, the feature vector for a given adjacent vertebra case is normalized with respect to the model developed for each grade by subtracting the mean and dividing by the standard deviation feature values for the corresponding grade. For each grade, the Euclidean distance from the normalized feature vector to each of cluster centers is computed. A nearest centroid approach is used for each  $K$ -means model as the metric for disc space narrowing assessment. Let  $H_0, H_1, H_2$ , and  $H_3$  denote the minimum distances from the cluster centers for the clustering models developed for grades 0–3, respectively. An intermediate disc space narrowing assignment used as a benchmark is given by assigning the grade  $i$  as  $i = \arg \min(H_i)$  for  $0 \leq i \leq 3$ .

### 2.8. Self-organizing map (SOM) method for disc space narrowing grade assignment

The second tier of the algorithm used Kohonen’s SOM [27] for grade assignment SOMs were used because the output mappings reflect the similarity of the feature data for the different classes. From the disc space narrowing grading system 0–3, disc space narrowing is more pronounced with increasing grade. Accordingly, there are similarities with vertebrae interfaces at consecutive grades such that interfaces labeled with grade 0 are similar to interfaces labeled with grade 1 but are less comparable to interfaces labeled grade 2. SOM was also chosen because of the asymmetric distribution of the data set with respect to the number of vertebra interfaces labeled for each grade. The inputs to the SOM are the minimum distance  $H_0-H_3$  found from the clustering models for each grade. For training the SOM, the first step was to determine the number of output nodes  $J$ .  $J$  was determined empirically based on the number of training adjacent vertebra interface cases and the number of grade assignment classes (4). The second step was to train the SOM and assign the  $J$  output nodes to the different grades. The clustering minimum distances  $H_0-H_3$  are generated for all training adjacent vertebra cases and are input to SOM. The resulting trained SOM and outputs generated from the SOM are used for making grade

assignments for the output nodes. For assigning a given output node  $i$  ( $1 \leq i \leq J$ ), the number of vertebra interface cases allotted to that node are determined for each grade. Let  $F_0, F_1, F_2$  and  $F_3$  denote the number of vertebra interface cases assigned to output node  $i$  for grades 0–3, respectively, from the training data. Because there are unequal numbers of adjacent vertebra interface cases for each grade, grade  $t$  ( $t = \{0, 1, 2, 3\}$ ) is assigned to output node  $i$  which yields the maximum ratio  $F_t/L_t$ , where  $L_t$  denotes the total number of vertebra interface cases in the training set for grade  $t$ . In other words, the grade assigned to output node  $i$  is specified as the grade that provides the greatest percentage of the vertebra interface training data that maps to output node  $i$ . This process is repeated for all  $J$  output nodes.

For the remaining test vertebra interfaces, the following procedure is performed for disc space narrowing grade assignment. First, the features  $M, O, P$  and  $R$  are computed. Second, the features are normalized using the means and standard deviations determined from the training data for each feature for each clustering model. Third, the distances  $H_0-H_3$  are computed using the clustering model for grades 0–3, respectively. Fourth, the disc space narrowing grade is determined from the output node assignment from the SOM network based on the inputs  $H_0-H_3$ .

### 3. Experiments performed

The disc space narrowing prediction algorithm is evaluated using the data set presented in Section 2.1. Twenty randomly generated training and test sets are generated for evaluating the features and disc space narrowing assignment techniques. For algorithm and feature evaluation, 80% of the vertebrae interfaces for each grade were used for training, and the remaining 20% of the vertebrae interfaces for each grade were used for test. For each training and test set,  $K$ -means clustering and SOM models are determined for disc space narrowing assignment.

Two schemes were examined for assigning disc space narrowing grades to the vertebrae interfaces from the experimental data set. For both methods, the same training and test sets were used for direct comparison of the algorithm results. The first approach involved training the  $K$ -means clustering model for each grade using the method presented in Section 2.7. For each vertebrae interface, the features  $M, O, P$  and  $R$  are computed and normalized for each of the clustering models. The grade corresponding to the minimum Euclidean distance from the cluster centers for the different grade models is assigned to the vertebrae interface. The second approach is the cascaded two-tier clustering and SOM algorithm presented in Section 2.8. For each vertebrae interface, the disc space narrowing grade assignment is made based on the grade label given to the SOM output mapping.

The automatically determined grades were compared to the truthed grade data, and percentage correct assignment was computed. Two schemes were examined for scoring the automatically determined grade assignments. In the first scheme, the predicted grade must match exactly with the truthed grade for the grade assignment to be deemed correct. For example, a vertebra interface called grade 1 by the automated algorithm is correct if the truthed grade for that vertebra interface is grade 1. The second scheme scores a vertebra interface grade prediction that is within one grade of the truthed grade as a correct grade assignment. For example, a vertebra interface with a predicted grade of 0 or 1 is scored as a correct grade assignment for a vertebra interface with a truthed grade of 0. However, predicting grades 2 or 3 for that vertebra interface would be called an incorrect grade prediction. The second scoring scheme was used because the four grades are not independent; the distinction between consecutive grade assignments is often being difficult to visually determine. Percentage correct grade assignment is determined for the training and test data sets using the two grade assignment and two scoring schemes described above. Average and standard deviation results are also generated for evaluation of the features and schemes presented.

### 4. Experimental results and discussion

Image analysis and clustering techniques are explored to predict disc space narrowing grades between adjacent vertebrae. Fig. 8 presents an image example of the algorithm used to determine the separator segment between adjacent vertebrae to facilitate feature calculations. Fig. 8(a) shows the adjacent filled vertebrae (connected component labeled). Fig. 8(b) gives the distance transform image after inverting the binary filled vertebrae image from (a). Note that histogram equalization was performed on the distance transform image for visualization. Fig. 8(c) provides the binary image with all pixels satisfying the Kirsch magnitude criterion ( $K(x, y) \geq 5$  for  $C_0 \leq x \leq C_1$  and  $R_0 \leq y \leq R_1$ ). Fig. 8(d) presents the thresholded separator image  $S$  that satisfies the Kirsch magnitude and direction criteria using the most frequently occurring direction  $\text{dir}_{\max}$ . Fig. 8(e) shows the closed binary separator image  $Z$  obtained from applying the morphological closing operation to  $S$  using a disk structuring element of radius 2. Fig. 8(f) gives the updated binary separator image  $B$  with the noise regions subtracted detected from  $Z$ . Fig. 8(g) presents the separator object between the adjacent vertebrae. Fig. 8(h) shows the separator object between the adjacent vertebrae contained within the outer edges of the vertebrae. The separator object shown in Fig. 8(h) is skeletonized to provide a mask for the distance transform image  $D$  to facilitate calculation of the features  $M, O, P$  and  $R$ .

Evaluation of the disc space narrowing grade prediction algorithms over 20 randomly generated training and test

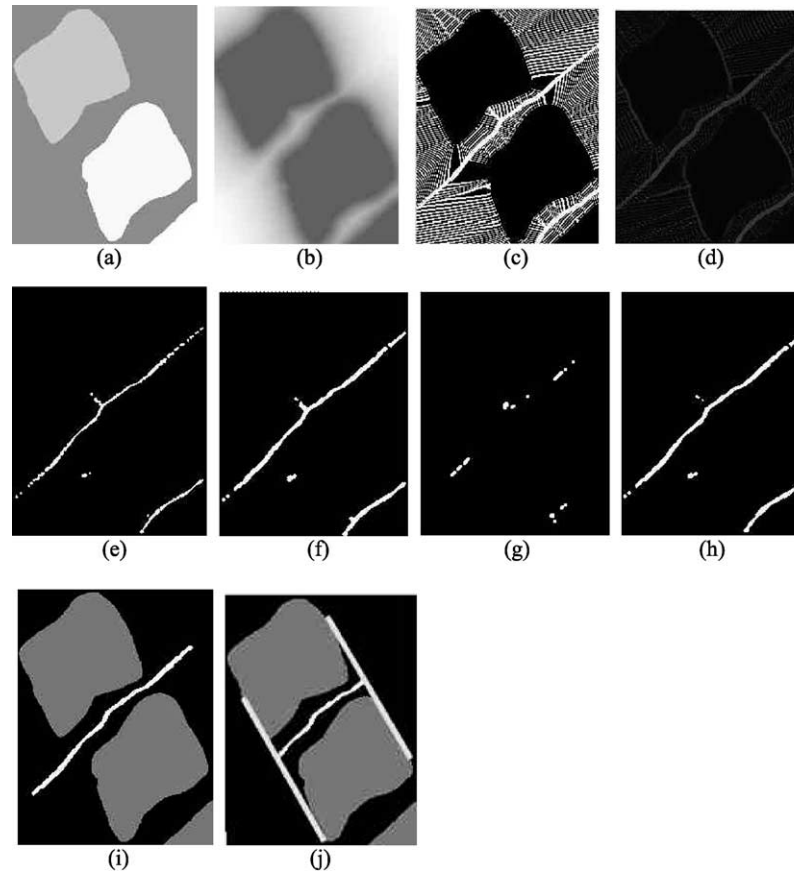


Fig. 8. Image example of the separator segment determination algorithm steps. (a) Filled adjacent vertebrae (connected component labeled). (b) Distance transform image after inverting the binary filled vertebrae image from (a) using histogram equalization for visualization. (c) Binary image containing all pixels satisfying edge magnitude criterion. (d) Thresholded image satisfying edge magnitude and direction criteria based on  $\text{dir}_{\max}$ . (e) Morphological closing of (d). (f) Binary image with noise regions removed from (e). (g) Vertebrae separator object. (h) Vertebrae separator object from (g) contained within the outer edges of the vertebrae.

sets. The two grade prediction algorithms examined include the  $K$ -means clustering model approach for each of the four grades and the two-tier SOM method. From empirical analysis, the number of clusters used for the  $K$ -means clustering to model each grade was determined as  $N_0 = 8$ ,  $N_1 = 10$ ,  $N_2 = 7$  and  $N_3 = 7$ , and the number of SOM outputs utilized was  $J = 45$ . Note that these parameters were used for all 20 randomly generated training/test sets. The following sections contain the experimental results from the two grade prediction techniques based on the exact grade and relaxed window of one grade scoring approaches.

#### 4.1. Disc space narrowing grade assignment results using $K$ -means clustering and nearest centroid approach

The average and standard deviation correct grade assignment results are tabulated in Table 2 for the training and test data using  $K$ -means clustering and nearest centroid grade prediction based on the exact grade criterion for the 20 randomly generated training and test sets. Columns 2–5 present the training results for grades 0–3. Columns 6–9 give the test results for grades 0–3. The mean and standard deviation of all the iterations are also provided. Table 3

provides a summary of the 20 randomly generated training and test grade assignment results using the  $K$ -means clustering and nearest centroid approach for grade assignment based on the relaxed window of one grade criterion. Column 1 shows the iteration number for the randomly generated training/test sets. Otherwise, Table 3 has the same column layout as Table 2 and also contains the mean and standard deviation of percentage correct grade assignment.

#### 4.2. Results using the two-tier approach for grade assignment

The average and standard deviation correct grade assignment results are presented in Table 4 for training and test data using the two-tier  $K$ -means and SOM technique based on the exact grade criterion for the 20 training/test sets. These experimental results are based on the same training and test sets as for the  $K$ -means clustering and nearest centroid approach presented in the previous section. Columns 2–5 present the training results for grades 0–3. Columns 6–9 give the test results for grades 0–3. Table 5 shows the training and test grade assignment results for the two-tier approach using the relaxed window of one

Table 2

Average and standard deviation correct training and test vertebrae interface grade prediction results using *K*-means clustering nearest centroid approach based on exact match criterion for 20 randomly generated training/test sets

	Training results (% correct)				Test results (% correct)			
	Grade 0	Grade 1	Grade 2	Grade 3	Grade 0	Grade 1	Grade 2	Grade 3
Mean	59.26	67.37	46.91	64.38	42.08	51.03	26.25	32.14
Standard deviation	10.17	5.19	6.36	7.62	18.91	10.09	12.44	10.95

Table 3

Percentage correct training and test vertebrae interface grade prediction results using *K*-means clustering nearest centroid approach based on window match criterion

Iteration number	Train results (% correct)				Test results (% correct)			
	Grade 0	Grade 1	Grade 2	Grade 3	Grade 0	Grade 1	Grade 2	Grade 3
1	89.36	94.83	95.74	83.33	100.00	96.55	83.33	42.86
2	97.87	91.38	93.62	83.33	100.00	82.76	91.67	42.86
3	91.49	92.24	93.62	70.83	83.33	100.00	100.00	42.86
4	93.62	96.55	95.74	87.50	91.67	89.66	100.00	28.57
5	89.36	89.66	97.87	95.83	75.00	96.55	100.00	85.71
6	93.62	96.55	91.49	83.33	100.00	93.10	83.33	71.43
7	95.74	95.69	91.49	75.00	100.00	93.10	91.67	42.86
8	97.87	93.10	93.62	75.00	100.00	93.10	91.67	71.43
9	93.62	88.79	89.36	70.83	100.00	100.00	100.00	57.14
10	91.49	93.97	95.74	79.17	91.67	86.21	91.67	71.43
11	95.74	93.97	95.74	83.33	91.67	89.66	100.00	57.14
12	93.62	96.55	91.49	95.83	83.33	86.21	91.67	42.86
13	95.74	96.55	93.62	87.50	91.67	96.55	83.33	57.14
14	93.62	96.55	95.74	87.50	83.33	96.55	100.00	28.57
15	91.49	91.38	95.74	79.17	100.00	89.66	91.67	71.43
16	97.87	93.97	87.23	62.50	100.00	89.66	100.00	71.43
17	91.49	93.97	91.49	79.17	100.00	96.55	83.33	57.14
18	93.62	92.24	89.36	91.67	91.67	93.10	91.67	57.14
19	95.74	96.55	85.11	75.00	100.00	89.66	83.33	71.43
20	91.49	98.28	91.49	75.00	100.00	96.55	91.67	71.43
Mean	93.72	94.14	92.77	81.04	94.17	92.76	92.50	57.14
Standard deviation	2.56	2.52	3.18	8.38	7.50	4.61	6.40	15.65

Results are shown for 20 randomly generated training/test sets with average and standard deviation.

grade criterion for the 20 training/test sets and the average and standard deviation for each grade. Column 1 shows the iteration number for the randomly generated training/test sets. Again, Table 5 has the same column layout as Table 4.

#### 4.3. Discussion of experimental results

There are several observations from Tables 2–5. First, the average correct grade assignment results for each grade

are much improved using the window scoring criterion over the exact grade match for the two-tier cascaded *K*-means and SOM approach and the *K*-means method (in isolation). For the *K*-means method, the improvements in the average grade assignment for the window criterion over the exact grade match are 52.09, 41.73, 66.25 and 25.00% for grades 0–3, respectively. For the two-tier approach, the improvements in the average grade assignment for the window criterion over the exact grade match are 24.17, 52.07, 62.08

Table 4

Average and standard deviation correct training and test vertebrae interface grade prediction results using two-tier *K*-means clustering and SOM approach based on exact match criterion for 20 randomly generated training/test sets

	Training results (% correct)				Test results (% correct)			
	Grade 0	Grade 1	Grade 2	Grade 3	Grade 0	Grade 1	Grade 2	Grade 3
Mean	79.26	42.67	52.34	78.75	66.25	33.10	31.67	52.86
Standard deviation	4.92	5.32	11.46	7.01	14.43	9.05	12.57	18.01

Table 5

Percentage correct training and test vertebrae interface grade prediction results using two-tier *K*-means clustering and SOM approach based on exact match criterion

Iteration number	Training results (% correct)				Test results (% correct)			
	Grade 0	Grade 1	Grade 2	Grade 3	Grade 0	Grade 1	Grade 2	Grade 3
1	89.36	80.17	95.74	100	83.33	75.86	100	85.71
2	93.62	89.66	97.87	100	91.67	86.21	91.67	85.71
3	82.98	78.45	95.74	95.83	75	79.31	100	100
4	95.74	88.79	95.74	100	83.33	82.76	91.67	57.14
5	91.49	87.07	89.36	100	91.67	93.1	91.67	100
6	91.49	86.21	91.49	100	91.67	89.66	91.67	85.71
7	89.36	87.93	97.87	100	91.67	79.31	91.67	71.43
8	93.62	86.21	97.87	91.67	91.67	79.31	75	100
9	89.36	85.34	95.74	100	58.33	89.66	100	85.71
10	93.62	83.62	93.62	95.83	91.67	79.31	91.67	100
11	91.49	81.03	95.74	95.83	83.33	75.86	100	100
12	91.49	91.38	93.62	91.67	100	82.76	100	71.43
13	91.49	86.21	91.49	100	100	89.66	100	71.43
14	93.62	90.52	91.49	100	83.33	82.76	91.67	85.71
15	87.23	83.62	95.74	100	100	93.1	91.67	85.71
16	89.36	85.34	97.87	95.83	100	93.1	91.67	42.86
17	95.74	87.93	95.74	100	100	96.55	100	71.43
18	89.36	87.07	93.62	95.83	100	82.76	100	100
19	89.36	89.66	97.87	95.83	100	93.1	91.67	71.43
20	89.36	90.52	95.74	100	91.67	79.31	83.33	71.43
Mean	90.96	86.34	95.00	97.92	90.42	85.17	93.75	82.14
Standard Deviation	3	3.55	2.52	2.87	10.57	6.53	6.55	15.97

Results are shown for 20 randomly generated training/test sets with average and standard deviation.

and 29.28% for grades 0–3, respectively. The exact grade criteria scoring results are poor, with low average assignments for grades 0–3 and high standard deviations. The disparity in the exact grade match and window grade criteria results highlights the similarities between consecutive grades. For truthing the vertebrae interface data, the expert radiologist used the grading scale developed by a group of Rheumatologists as part of the Online Digital Atlas Version 2.0. There is no discrete transition from one grade to the next in evaluating disc space narrowing. For example, Fig. 9 provides an image example of a vertebrae interface (C3–C4) with truthed grade 0 by the radiologist, but was assigned grade 1 by the two-tier algorithm. Note that this vertebrae interface would be correctly assigned using the sliding window scoring criterion. The grading system is used to represent the degree of disc narrowing presence at vertebrae interfaces. The distinction between slight and significant degrees of disc space narrowing is important information that can be used for patient diagnosis and treatment.

The second observation is that the *K*-means clustering approach (in isolation) yields comparable average correct grade assignment to the two-tier method for grades 0–2 using the window scoring criterion. From Table 3, the average correct grade assignment rates for the *K*-means approach are 94.17, 92.76, 92.5 and 57.14% for grades 0–3, respectively. From Table 5, the average correct grade assignment rates for the two-tier method are 90.42, 85.17,

93.75 and 82.14%, respectively. The average correct results for the *K*-means approach are higher for grades 0 and 1 than for the two-tier method. However, the two-tier method has much higher average correct results for grades 2 and 3, particularly grade 3, than for the *K*-means approach (in isolation). The *K*-means approach simply assigns the grade based on the minimum distance from the four *K*-means models. This approach does not account for the similarity between grades. The minimum distance from the *K*-means clustering models are the inputs to the SOM component of the two-tier method. The SOM maps the output nodes to reflect the similarity of consecutive grades. There are many more vertebrae interfaces with truthed grade 1 (159) than



Fig. 9. Example of vertebrae interface missed using exact match criterion. The vertebrae interface is truthed as grade 0 but called grade 1 by the two-tier algorithm.

with grade 3 (31). The difference in the number of training cases impacts the training of the clustering approaches for vertebrae interface labeling. The third observation is that the standard deviation experimental results for the exact match and the window scoring criteria are relatively high, particularly for grade 3. The high standard deviations show some degree of inconsistency of the features used for grade assignment. The disparity in the number of vertebrae interfaces for each grade in the data set affects the training of the algorithms used for grade assignment. The purpose for using the clustering techniques, *K*-means and SOM, was to attempt to compensate for this disparity.

The final observation is that the scale invariant features investigated can be successfully applied to vertebrae interface grade assignment using the window scoring criteria. From Table 5, the two-tier approach yielded 90.42, 85.17, 93.75 and 82.14% for grades 0–3 for the window scoring criterion. The four features investigated attempt to quantify the spacing between adjacent vertebrae relative to the size of those adjacent vertebrae. The expert radiologist examined the region of greatest constriction, i.e. minimum distance between adjacent vertebrae, along with the Online Atlas guide for grade assignment. The features examined attempted to mimic the approach used by the radiologist for vertebrae interface grade assignment.

## 5. Summary

This research introduces computer assisted techniques for characterizing disk space narrowing. Four scale invariant features were presented and evaluated using clustering techniques. A four grade scale was used for disc space narrowing assessment. Increased vertebrae interface grade assignment indicates more disc space narrowing, with grade 0 representing normal spacing and grade 3 indicating significant disc space narrowing. Accordingly, vertebrae interfaces do not significantly change for consecutive grade assignments. Using a two-tier *K*-means and SOM approach with a window of one grade for scoring yielded average test grade assignments of greater than 82.00% for all grades. The experimental results demonstrate the potential for computer assisted techniques for categorizing disc space narrowing.

## References

- [1] Fact Sheet: Osteoarthritis. American College of Rheumatology, Atlanta, GA; 1994.
- [2] Disease statistics: Fast Facts, website for the National Osteoporosis Foundation, [www.nof.org/osteoporosis/stats.htm](http://www.nof.org/osteoporosis/stats.htm); May 2003.
- [3] Long LR, Thoma GR. Image query and indexing for digital X-rays. SPIE Conference on Storage and Retrieval for Image and Video Databases VII, San Jose, CA. Proceedings of SPIE 1999;3656: 12–21.
- [4] Hedlund LR, Gallagher JC. Vertebral morphometry in diagnosis of spinal fractures. *Bone Miner* 1988;5:59–67.
- [5] Gallagher JC, Hedlund LR, Stoner S, Meeger C. Vertebral morphometry: normative data. *Bone Miner* 1988;4:189–96.
- [6] Minne HW, Leidig G, Wuster C, Siromachkostov L, Baldauf G, Bickel R, Sauer P, Lojen M, Ziegler R. A new developed spine deformity index (SDI) to quantitate vertebral crush fractures in patients with osteoporosis. *Bone Miner* 1988;3:335–49.
- [7] Raymakers JA, Kapelle JW, van Beresteijn ECH, Duursma SA. Assessment of osteoporotic spine deformity: a new method. *Skeletal Radiol* 1990;19:91–7.
- [8] Eastell R, Cedel SL, Wahner HW, Riggs BL, Melton LJ. Classification of vertebral fractures. *J Bone Miner Res* 1991;6: 207–15.
- [9] McCloskey EV, Spector TD, Eyres KS, Fern ED, O'Rourke N, Vasikaran S, Kanis JA. The assessment of vertebral deformity: a method for use in population studies and clinical trials. *Osteoporosis Int* 1993;3:138–47.
- [10] Saur P, Leidig G, Minne HW. Spine deformity index (SDI) versus other objective procedures of vertebral fracture identification in patients with osteoporosis: a comparative study. *J Bone Miner Res* 1991;6:227–38.
- [11] Smith-Bindman R, Cummings SR, Steiger P, Genant HK. A comparison of morphometric definitions of vertebral fracture. *J Bone Miner Res* 1991;6:25–34.
- [12] Ross PD, Davis JW, Epstein RS, Wasnich RD. Ability of vertebral dimensions from a single radiograph to identify fractures. *Calcif Tissue Int* 1992;51:95–9.
- [13] Ott SM, Kilocyne RF, Chesnut III CH. Ability of four different techniques of measuring bone mass to diagnose vertebral fractures in postmenopausal women. *J Bone Miner Res* 1987;2:201–10.
- [14] Kleerekoper M, Parfitt AM, Ellis BL. Measurement of vertebral fracture rates in osteoporosis. *Proc Copenhagen Int Symp Osteoporosis* 1984;103–9.
- [15] Barnett E, Nordin BEC. The radiological diagnosis of osteoporosis: a new approach. *Clin Radiol* 1960;11:166–74.
- [16] Genant HK, Ettinger B, Harris ST, Block JE, Steiger P. Quantitative computed tomography in assessment of osteoporosis. In: Riggs BL, Melton LJ, editors. *Osteoporosis: etiology, diagnosis and management*. New York, NY. 1988. p. 221–49.
- [17] Mazess RB, Wahner HM. Nuclear medicine and densitometry. In: Riggs BL, Melton LJ, editors. *Osteoporosis: etiology, diagnosis and management*, New York, NY. 1988. p. 251–95.
- [18] Sartoris DJ, Resnick D. Dual energy radiographic absorptiometry for bone densitometry: current status and perspective. *AJR* 1989;152: 242–6.
- [19] Kalifa G, Cohen PA, Hamidou A. The intervertebral disk: a landmark for spinal diseases in children. *Eur Radiol* 2002;12(3):660–5.
- [20] Paajanen H, Erkintalo M, Parkkola R, Salminen J, Kormanen M. Age-dependent correlation of low-back pain and lumbar disc regeneration. *Arch Orthop Trauma Surg* 1997;116(1–2):106–7.
- [21] Miller JA, Schmatz C, Schultz AB. Lumbar disc degeneration: correlation with age, sex and spine level in 600 autopsy specimens. *Spine* 1998;13(2):173–8.
- [22] Hamalainen O, Vanharanta H, Kuusela T. Degeneration of cervical intervertebral disks in fighter pilots frequently exposed to high + Gz forces. *Aviat Space Environ Med* 1993;64(8):692–6.
- [23] Lu J, Ebraheim NA, Huntoon M, Haman SP. Cervical intervertebral disc space narrowing and size of intervertebral foramina. Department of Orthopaedic Surgery, Medical College of Ohio, Toledo. *Clin Orthopaedics Related Res* 2000;370:259–64.
- [24] Gale DR, Chaisson CE, Totterman SM, Schwartz RK, Gale ME, Felson D. Meniscal subluxation: association with osteoarthritis and joint space narrowing. *Osteoarthritis Cartilage* 1999;7(6):526–32.
- [25] Long LR, Pillemer SR, Goh G-H, Berman LE, Neve L, Thoma GR, Premkumar A, Ostchega Y, Lawrence RC, Altman RD, Lane NE,

- Scott Jr. WW. A digital atlas for spinal X-rays. Newport Beach, CA. Proc SPIE Med Imaging : PACS Des Eval 1997;3035:586–94.
- [26] The Department of Rheumatology and Medical Illustration and Manchester Royal Infirmary and the Empire Rheumatological Council's Field Unit, The Epidemiology of Chronic Rheumatism. Atlas of standard radiographs of arthritis, vol. II. Philadelphia, PA: F.A. Davis Company; 1963.
- [27] Stanley RJ, Long R. A radius of curvature-based approach to cervical spine vertebra image analysis. Copper Mountain, CO. Proc 38th Annu Rocky Mountain Bioengng Symp 2001;37:385–90.
- [28] Tsai MD, Jou SB, Hsieh MS. A new method for lumbar herniated inter-vertebral disc diagnosis based on image analysis of traverse sections. *Comput Med Imaging Graphics* 2002;26(6):369–80.
- [29] Duryea J, Li J, Peterfy CG, Gordon C, Genant HK. Trainable rule-based algorithm for the measurement of joint space width in digital radiographic images of the knee. *Med Phys* 2000;27(3): 580–91.
- [30] Zhang Z, Stoecker WV, Moss RH. Border detection of digitized skin tumor images. *IEEE Transact Med Imaging* 2000;19(11): 1128–43.
- [31] Kirsch R. Computer determination of the constituent structure of biological images. *Comput Biomed Res* 1971;4:315–28.
- [32] Haralick RM, Shapiro LG. *Comput Robot Vision*; 1992.
- [33] Serra J. *Image analysis and mathematical morphology*. New York: Academic Press; 1982.
- [34] Rosenfeld A, Pfaltz JL. Sequential operations in digital picture processing. *J Assoc Comput Machinery* 1966;13:471–94.
- [35] Zurada JM. *Introduction to artificial neural systems*. New York: West Publishing Co; 1992.
- [36] Kohonen T. Self-organized formation of topologically correct feature maps. *Biol Cybern* 1982;43:59–69.

**Pavan Chamarthy** received a Bachelor of Technology degree in Electronics and Communication Engineering in 1997 from JNTU College of engineering, Hyderabad. He is completing his MS degree in Electrical Engineering at the University of Missouri Rolla.

**R. Joe Stanley** received the BSEE and MSEE degrees in electrical engineering and a PhD degree in Computer Engineering and Computer Science from the University of Missouri-Columbia. As a graduate student at the University of Missouri-Columbia, he worked under training grants from the National Library of Medicine and the National Cancer Institute. Upon completing his doctoral study, he served as Principal Investigator for the Image Recognition program at Systems and Electronics, Inc. in St Louis, MO. He is currently an Assistant Professor in the Department of Electrical and Computer Engineering at the University of Missouri-Rolla. His research interests include signal and image processing, pattern recognition and automation. Dr Stanley is a Senior Member of the IEEE and a member of NAFIPS.

**Gregory Cizek** has a degree in bio-medical engineering from Northwestern University and a medical degree from Washington University. He did his residency in diagnostic radiology at the University of Chicago and a neuroradiology fellowship at Barnes Hospital. Dr Cizek has been a licensed physician since 1990 and currently is the chairman of the Department of Radiology at Des Peres Hospital in St Louis, MO and runs an imaging and spine care outpatient center in St Louis. Dr Cizek performs all aspects of radiology with a special interest in the spine including spinal procedures. He is a member of several spine societies (N. American Spine Society, International Spinal Injection Society) and is a radiology consultant to the spinal hardware division of Medtronic.

**L. Rodney Long** is an electronics engineer for the Communications Engineering Branch in the Lister Hill National Center for Biomedical Communications, a research arm of the National Library of Medicine. He has held his current position since 1990. Prior to his current job, he worked for 14 years in industry as a software developer and as a systems engineer. His research interests are in image processing and scientific/biomedical databases, with emphasis on the content-based retrieval of medical images. He has an MA in applied mathematics from the University of Maryland.

**Sameer Antani** is with the Lister Hill National Center for Biomedical Communications at the National Library of Medicine. He earned his BE (Computer) degree from the University of Pune, India, in 1994; and ME and PhD degrees in Computer Science and Engineering from The Pennsylvania State University in 1998 and 2001, respectively. He is interested in Content Analysis of Visual Information, Multimedia Databases, Medical Image Databases, Computer Vision, Document Image Analysis, and Computer Graphics. His current projects include topics on (complete and partial) shape representation and similarity algorithms for spine X-ray image retrieval, color- and texture-based segmentations of acetowhitened images of the uterine cervix, and image indexing algorithms, among others. Sameer is a member of the IEEE and the IEEE Computer Society.

**George R. Thoma** is Chief of the Communications Engineering Branch of the Lister Hill National Center for Biomedical Communications, a research and development division of the US National Library of Medicine. In this capacity, he directs R&D programs in document image analysis and understanding, biomedical image processing, image compression, automated document image delivery, digital X-ray archiving, animated virtual books, and high speed image transmission. He earned a BS from Swarthmore College, and the MS and PhD from the University of Pennsylvania, all in electrical engineering. Dr Thoma is a Fellow of the SPIE, the International Society for Optical Engineering.